

Charge State Control of F₁₆CoPc on *h*-BN/Cu(111)

Mathias Pörtner, Yinying Wei,* Alexander Riss, Knud Seufert, Manuela Garnica, Johannes V. Barth, Ari P. Seitsonen, Lars Diekhöner, and Willi Auwärter*

The use of molecular materials in solar cells and nano-electronics demands a fundamental understanding and control of their electronic properties. Particularly relevant is the molecular response to the environment, that is, the interaction with the support and adjacent molecules, as well as the influence of electrostatic gating. Here, the control of molecular level alignment and charge states of fluorinated cobalt phthalocyanines (F₁₆CoPc) on atomically thin hexagonal boron nitride (*h*-BN) sheets on Cu(111) is reported using scanning tunneling microscopy (STM) and spectroscopy (STS), as well as atomic force microscopy (AFM) and complementary density functional theory (DFT) calculations. Three parameters that govern the electronic level alignment of F₁₆CoPc orbitals are investigated: i) template-induced gating by the work function variation of the *h*-BN/Cu(111) substrate, ii) gating by the STM tip, and iii) screening by neighboring molecules. The interplay of these parameters influences the charge distribution in the studied molecular arrangements and thus provides the possibility to tune their physicochemical behavior, for instance, the response toward electronic or optical excitation, charge transport, or binding of axial adducts.

nano-electronics, sensing, and quantum science.^[1–4] Their integral performance characteristics depend notably on the molecular constituents and their interactions with each other. Furthermore, the influence of the substrate, and the response to external stimuli, such as an applied electric field, can play a major role. Control of the macroscopic properties of such hybrid materials thus relies on a fundamental microscopic understanding of the electronic properties of the molecular building blocks within their environment.^[5,6] Atomic-scale studies of molecular behavior have been extensively performed on metal substrates,^[7,8] due to the facile application of STM and STS. However, the electronic interaction of the molecules with metals often leads to considerable hybridization which can mask or adversely affect the intrinsic properties of the molecules. Thin films of decoupling layers with a band gap or low density of

1. Introduction

The modification of the molecular electronic structure at interfaces—affected through level alignment, charging, and charge transfer—by gating and screening is highly relevant for potential applications of molecular materials in solar cells,

states around the Fermi energy grown on metal surfaces^[9–13] reduce the interaction between the substrate and the molecular adsorbates but retain the possibility to perform STM/STS measurements. A particularly useful decoupling layer is one-atom-thick hexagonal boron nitride (*h*-BN). *h*-BN layers are chemically inert, exhibit high temperature stability, and importantly, can be grown as full monolayers on metallic substrates, thus providing a suitable substrate for molecular adsorption.^[12] Molecular adsorbates have been shown to be influenced by the work function modulation of such substrates (which is associated with the formation of a moiré pattern^[12,14]), the screening by the substrate^[15–17] and by neighboring molecules,^[18–20] as well as electric fields applied via back^[21,22] and top gating.^[23,24] Such effects—which can be strongly influenced by the molecular density—can entail changes in the physicochemical characteristics of the molecules, such as charging^[22–26] and conformational or chemical switching.^[27] To achieve full control of the molecular response, a detailed understanding of the complex interplay of these effects is thus needed.

Dr. M. Pörtner, Dr. A. Riss, Dr. K. Seufert, Dr. M. Garnica, Prof. J. V. Barth, Prof. W. Auwärter
 Physics Department E20
 Technical University of Munich
 Garching D-85748, Germany
 E-mail: wau@tum.de

Dr. Y. Wei, Prof. L. Diekhöner
 Department of Materials and Production
 Aalborg University
 Aalborg DK-9220, Denmark
 E-mail: yinyingwei7@gmail.com

A. P. Seitsonen
 Département de Chimie
 École Normale Supérieure
 Paris F-75005, France

 The ORCID identification number(s) for the author(s) of this article can be found under <https://doi.org/10.1002/admi.202000080>.

© 2020 The Authors. Published by WILEY-VCH Verlag GmbH & Co. KGaA, Weinheim. This is an open access article under the terms of the Creative Commons Attribution-NonCommercial License, which permits use, distribution and reproduction in any medium, provided the original work is properly cited and is not used for commercial purposes.

Fluorinated metal phthalocyanines have been intensively studied as stable building blocks for organic semiconductor applications, providing large ionization potentials.^[28–30] Specifically, interfacial electronic properties with F₁₆CoPc adsorbed on metals, organic films, and 2D materials were addressed, revealing the electron acceptor character of the molecule, including charge transfer from the support to the Co center.^[30,31]

Here we show how the molecular energy level alignment and the charge state of F₁₆CoPc molecules on *h*-BN/Cu(111)

DOI: 10.1002/admi.202000080

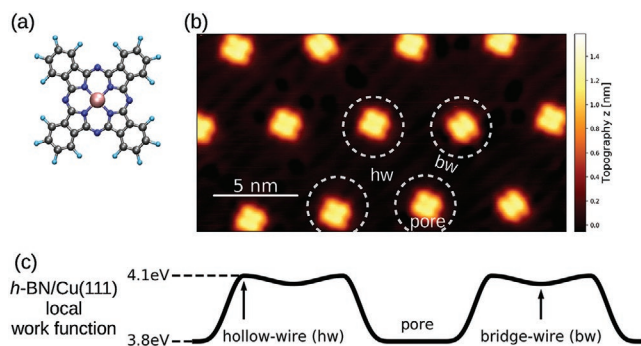


Figure 1. Preferential adsorption of F₁₆CoPc on h-BN/Cu(111). a) Chemical structure model of F₁₆CoPc (light blue:fluorine, gray:carbon, dark blue:nitrogen, pink:cobalt). b) STM image of 0.06 ML F₁₆CoPc on h-BN/Cu(111) ($V_S = 1$ V, $I = 38$ pA). Dashed white circles mark the pore areas of the h-BN/Cu(111) moiré superstructure. The two types of wire regions are labeled with “hw” (hollow-wire) and “bw” (bridge-wire). c) Schematic illustration of the local work function modulation of h-BN/Cu(111), varying by 0.3 eV between the hollow-wire and the pore areas.^[14]

are controlled by three crucial parameters: i) the template-induced gating due to the moiré-induced spatial variation of the substrate electronic landscape,^[12,14] ii) gating by the STM tip,^[22–24,32–34] and iii) the screening by neighboring molecules.^[16,18] A combination of these parameters can cause a change in the molecular charge state of F₁₆CoPc on h-BN/Cu(111), that is, a shift of frontier orbitals across the Fermi level (E_F), which can be associated with sharp features in the dI/dV spectra. In addition, AFM measurements, which provide a way to probe charge transfer effects at larger distances (even when the tunneling current is below the detection threshold) reveal the occurrence of multiple simultaneous charge state changes due to tip-induced gating. Compared to template- and tip-induced gating as well as screening by neighboring molecules, charge state changes of adjacent molecules were found to exert a much smaller influence on the molecular level alignment.

2. Results and Discussion

Deposition of 0.06 ML of F₁₆CoPc (Figure 1a) onto h-BN/Cu(111) held at room temperature and subsequent cooling to 5 K results in the formation of a superlattice from isolated molecules. As seen in Figure 1b, the molecules preferentially occupy the pore areas of the moiré pattern—reflecting the lattice mismatch of the h-BN layer and the underlying Cu(111) substrate—where the surface potential is lower.^[12,14] The alignment of F₁₆CoPc on the h-BN/Cu(111) support is described in Section S1, Supporting Information.

2.1. Template-Induced Gating

The electronic landscape modulation of the substrate—the pore areas exhibit a 0.3 eV lower local work function than the wire areas (Figure 1c)—is reflected in the molecular level alignment as probed by dI/dV spectroscopy. Spectra of molecules adsorbed on the pore areas (Figure 2a) are shown in Figure 2d–f. In all cases a pronounced occupied-states feature

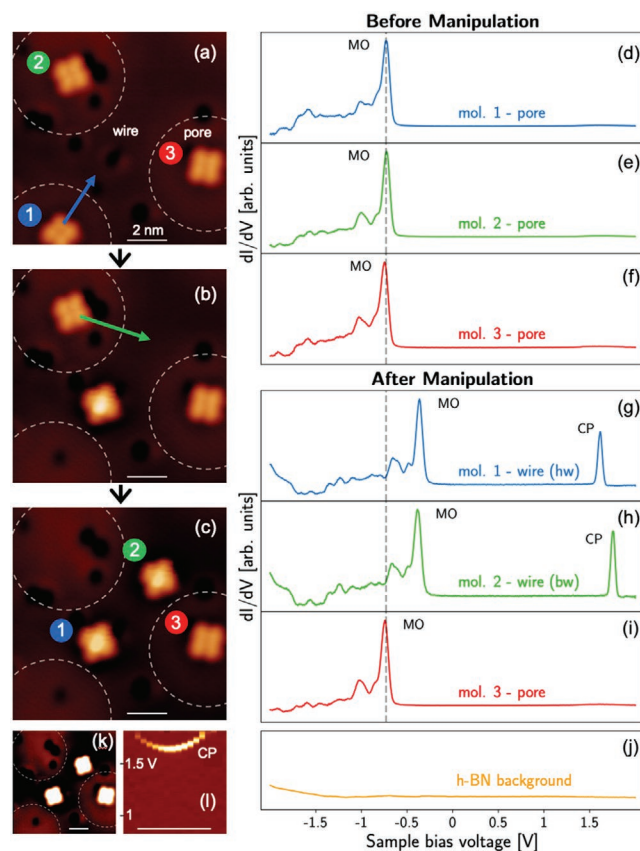


Figure 2. Template-induced gating of individual F₁₆CoPc molecules. a) Three molecules adsorbed on moiré pore sites (dashed white circles). b) Molecule 1 (blue) was moved from the pore to a hollow-wire region by lateral STM manipulation. c) Molecule 2 (green) was moved from the pore to a bridge-wire region. d–f) dI/dV spectra of the three molecules before manipulation, that is, adsorbed on the pore regions as shown in (a), show electronic resonances associated with a molecular orbital (“MO”) at $V_S = -0.73$ V. g–i) dI/dV spectra after manipulation. The energies of the molecular resonances are shifted for the molecules 1 and 2 to -0.36 and -0.38 V. In addition, charging peaks (“CP”) appear at $V_S > 1.5$ V in the spectra for molecules 1 and 2. j) Reference dI/dV spectrum taken on the h-BN substrate. k) Representation of the STM image in (c) with increased contrast to highlight the moiré superstructure. l) Exemplary dI/dV versus distance map along a path crossing a F₁₆CoPc, showing the parabola-like dependence of the CP’s energy on the lateral tip position. The full data set including explanation is available in Section S3, Supporting Information. Scan and dI/dV stabilization parameters: $V_S = 1$ V, $I = 29$ pA. Spectra in (d)–(i) were taken with the tip positioned above the centers of the molecules and normalized for better comparability. The dI/dV maximum ranges from 0.45 to 0.89 nS in spectra (d)–(f) and amounts to 0.06 nS in (j). The lateral manipulation was performed with $V_S = 50$ mV, $I = 0.3$ nA. All scale bars represent 2 nm.

at $V_S = -0.73$ V (labeled “MO,” molecular orbital) can be seen, while the unoccupied-states region at positive sample bias appears rather featureless when probed above the molecular center. The asymmetry of this MO peak is due to side peaks at $V_S < -0.73$ V, which likely originate from vibronic excitations of the electronically decoupled molecules.^[21,23,35–37] The resonance is tentatively assigned to a MO of the free molecule, which is occupied upon adsorption resulting in negatively charged molecules. As discussed later, this orbital has Co d_{z^2}

character. Indeed, a DFT-based modeling of the $F_{16}CoPc/h\text{-BN}/Cu(111)$ interface shows charge transfer toward the molecule that occurs in an anion state (see Paragraph 2.5 and Section S2, Supporting Information).

Lateral manipulation with the STM tip allows repositioning of the molecules from the pore regions (Figure 2a) to different areas of the moiré pattern. In the first step molecule “1” (Figure 2a) was moved to a hollow-wire site (Figure 2b). Then molecule “2” was moved to a bridge-wire site (Figure 2c), while molecule “3” in Figure 2a remained at its position at the pore region. This repositioning of the molecules gave rise to changes in the intramolecular resolution. Before manipulation, each of the three molecules exhibited fourfold symmetry and comparable apparent height. After manipulation, brighter centers can be seen for the repositioned molecules 1 and 2. The respective dI/dV spectra are shown in Figure 2g–i: The signatures of molecules 1 and 2 exhibit marked shifts of the “MO” peak from -0.73 to -0.36 V and -0.38 V, respectively (Figure 2g,h). This response agrees well with the change of the local work function across the moiré pattern (~ 0.3 eV),^[14,20,38] analogous to other $h\text{-BN}/\text{metal}$ templates.^[12,39] In agreement, our DFT calculations confirm an upshift of the molecular orbitals when placing $F_{16}CoPc$ on a wire area (mimicked by a B “on top” and N “on fcc” registry of $h\text{-BN}/Cu(111)$ ^[40] instead of adsorption on a pore area (B “on fcc” and N “on top” registry). The calculations also show that the local work function is increased by 0.53 eV with a single $F_{16}CoPc$ adsorbed, both on the pore and the wire areas (see Section S2, Supporting Information).

2.2. Tip-Induced Gating

In addition to the MO’s shift, a sharp peak (denoted “CP,” charging peak) appears at $V_S = 1.61$ V and $V_S = 1.76$ V in the spectra of the repositioned molecules 1 and 2, respectively. dI/dV maps taken above the respective energies associated with charging peaks show sharp ring-like features around the molecular center (see Sections S3 and S4, Supporting Information), analogous to what has been observed for charging of other adsorbates.^[22–26,32–34,41] The radii of these rings strongly depend on the applied bias, as well as on the tip height. Figure 2l displays a series of dI/dV spectra recorded along a path crossing a molecule, revealing a parabola-like behavior of the “CP” feature, with the energy position increasing with increasing tip distance from the center of the molecule. The “CP” is thus assigned to an electronic transition induced by the electric field between tip and sample, which causes a shift of the molecular levels across E_F .^[22–24,26,32–34] This process involves the MO introduced above. The position of the charging peak is directly proportional to the energetic position of the molecular orbital (see Section S5, Supporting Information). This can be described by estimating the voltage drops between tip and molecule, and molecule and the metallic substrate, respectively. According to this double barrier tunneling junction (DBTJ) model,^[18,23–25,32,33,37,42–44] the proportionality between the positions of the charging and MO peaks is given by $V_{CP}/V_{MO} = \epsilon z/d$,^[23,25,32,34] where z is the tip-molecule separation, d is the distance between the molecule and the $Cu(111)$ substrate, and ϵ is the dielectric constant associated with the molecule- $Cu(111)$ tunneling barrier including

the $h\text{-BN}$. In our measurements we found a proportionality $V_{CP}/V_{MO} = -4.8$ (see Section S5, Supporting Information). This means, that the initial unperturbed position of the MO will have a large impact on the bias threshold for the charge transition.

2.3. Screening

Further STM manipulation procedures show how the measured energy of the MO peak is affected by screening by neighboring molecules. For these experiments, we increased the molecular coverage, resulting in aggregates in the pore regions (cf. Section S6, Supporting Information).^[12,14] The dI/dV spectrum taken on the central molecule within a cluster of three molecules shows a molecular resonance at -0.67 V (Figure 3a). Subsequent removal of its left neighbor (Figure 3b) and its right neighbor (Figure 3c) by STM manipulation shifts the position of the MO of the central molecule each time by 40–50 mV toward more negative energies, that is, away from E_F . This energy shift can be explained by reduced screening of the transiently charged central molecule by neighboring molecules. The polarization energy of a molecule i can be quantified by

$$E_i^P = \frac{\alpha e^2}{4\pi\epsilon_0} \sum_{j \neq i} R_{ij}^{-4} \quad (1)$$

and depends strongly on the distance R_{ij} to all surrounding molecules j .^[18] e is the elementary charge and ϵ_0 is the vacuum permittivity. Considering only in-plane polarization, the polarizability tensor α can be approximated by a scalar for the C_4 -symmetric $F_{16}CoPc$ molecules. Based on calculated values for phthalocyanine molecules, we use an estimate of the $F_{16}CoPc_4$ polarizability of $\alpha = 137 \text{ \AA}^3$.^[45] The calculated polarization energies (empty circles) and the measured shifts of the MO peaks (filled markers) are plotted in Figure 3d for a dimer, trimer, and a molecular island, shown in the inset of Figure 3d. For those molecules in the island, polarization effects can cause large shifts of MO energies of a few hundred meV, in agreement with reports on a related system.^[18] Despite the simplicity and limitations of the applied model, it nicely reflects the values and trends observed in the experiment (see discussion paragraph below). Discrepancies between experiment and calculation, which are particularly evident for some of the investigated molecules in the island, can occur due to the template-induced gating (as discussed above). The gating effect is not taken into account in the calculation. For instance, molecule C6 is located close to a wire site causing an additional template-induced shift toward positive energies in the experimental data.

2.4. High Coverage Effects

At higher coverages, the molecules do not only adsorb at the preferred pore sites of the moiré lattice, but also at the wire regions (cf. Section S6, Supporting Information). The STM image of a surface with ~ 0.9 ML molecular coverage in Figure 4a recorded at 1 V reveals a brighter appearance of molecules adsorbed at wire regions compared to the ones adsorbed at pore regions. This difference in contrast can be understood by analyzing the dI/dV spectra of the molecular layer. Figure 4b

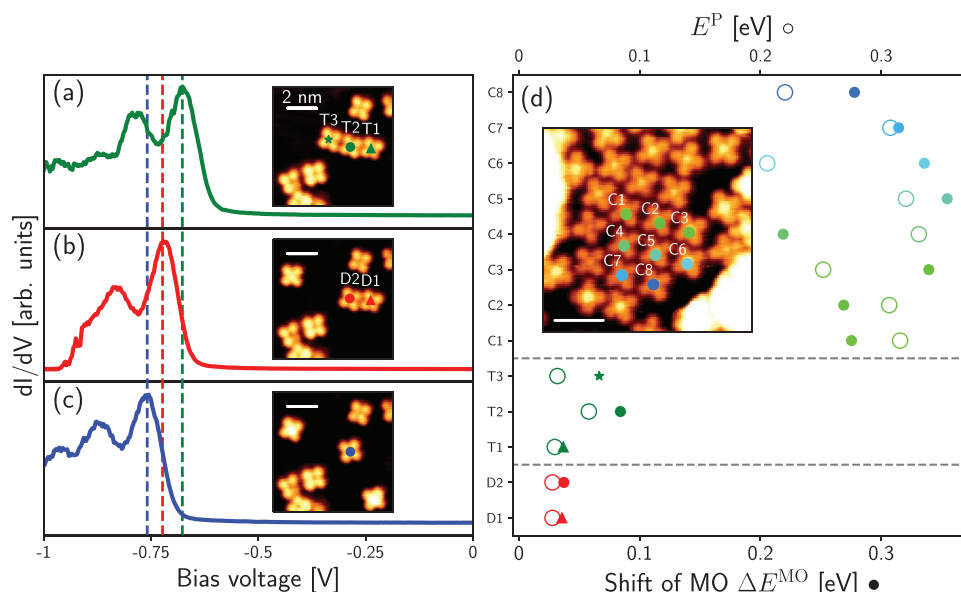


Figure 3. Energy shift of the MO peaks due to polarization. a–c) Removal of neighboring molecules by molecular manipulation causes a 40–50 mV decrease of the MO position for the central molecule in the dI/dV measurements (tip stabilization parameters: $V_S = 1$ V, $I = 50$ pA). d) Comparison of calculated polarization energies (empty circles, top x-axis) and measured shifts of MO peak energies with respect to an isolated $F_{16}CoPc$ (filled markers, bottom x-axis) for molecules in different assemblies: a cluster of two molecules (D1, D2), a cluster of three molecules (T1–T3), and an island of molecules (C1 to C8, see STM image in the inset ($V_S = 1$ V, $I = 50$ pA)) (Tip stabilization parameters for dI/dV spectroscopy: $V_S = 1$ V, $I = 20$ pA, scalebars: 2 nm).

shows spectra taken along the solid blue line in Figure 4a, in which the color-coded dI/dV intensity is plotted as a function of position (x -axis) and bias voltage (y -axis). The color plot shows separated features along the x -axis, which correspond to the eight molecules along the line. Representative dI/dV spectra for each of these molecules are shown in Figure 4c, in which the molecular resonances and the charging peaks are labeled

as “MO” and “CP”, respectively. In the color plot, the charging-related features (red dots in Figure 4b) exhibit sharp parabolic-like characteristics due to their strong energy-dispersion (cf. Figure 2l; Figure S4, Supporting Information), while the molecular resonances (blue dots in Figure 4b) give rise to a broader intensity distribution with side peaks. The energies of the MO peaks depend on the spatial position of the respective molecule

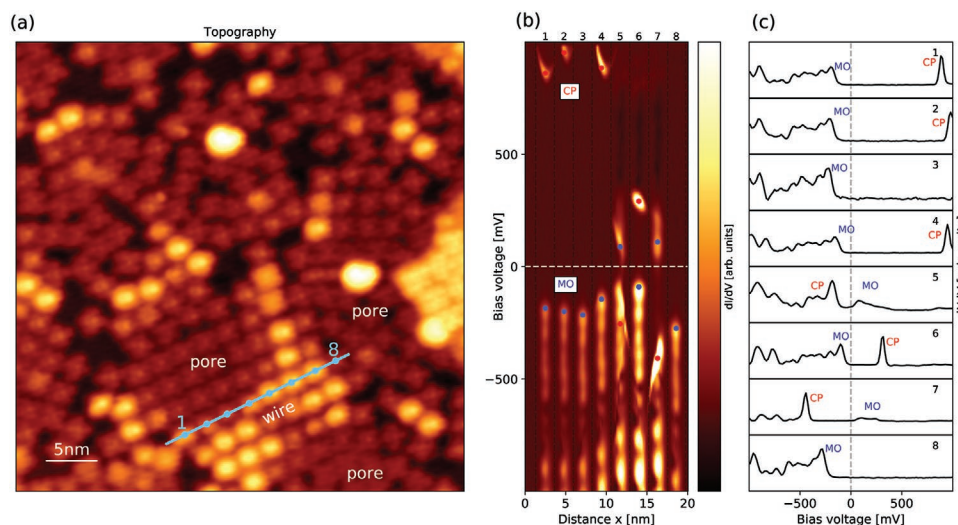


Figure 4. Template-induced shift of molecular levels, screening and charge state change for a sample with high $F_{16}CoPc$ coverage. a) STM image of $F_{16}CoPc$ at 0.9 ML coverage ($V_S = 1$ V, $I = 20$ pA). b) Visualization of the color coded intensity of dI/dV spectra along the light blue line in (a) as a function of lateral position (x -axis) and bias voltage (y -axis). The positions of the molecular resonances and charging features are marked with blue and red dots, respectively (tip stabilization parameters: $V_S = 1$ V, $I = 20$ pA). c) Representative dI/dV spectra taken close to the center of each of the eight molecules. The spectra show molecular resonances, the energies of which are affected by the modulation of the h -BN/Cu(111) work function and screening by the neighboring molecules. For the molecules with MO peaks sufficiently close to E_F , charging peaks at the opposite polarity are observed.

on the moiré superlattice, that is, template-induced gating (see Figure 1c) and on the molecular environment due to screening. For molecules 1, 2, 4, 5, 6, and 7, which exhibit MO energies close to E_F , charging peaks are observed at the opposite polarity of the MO peaks.^[22–24,26,33,34] The ratios between the absolute positions of the MO and CP remain at $|V_{CP}|/|V_{MO}| \approx 5$, regardless whether the CP is observed at occupied or unoccupied states. The MO and charging peak positions in the spectra for molecule 6 show a deviation from the expected behavior based on the *h*-BN/Cu(111) work function modulation, which points to potential additional effects (such as electrostatic interactions between the peripheries of the molecules or subtle variations of the adsorption height).^[46,47] Furthermore, impurities in the substrate might play a role.

The appearance of the molecules in Figure 4a is directly related to their respective spectra (Figure 4b,c). The molecules 1, 5, 6, 7 appear bright in the image because—at the applied imaging conditions—their MOs are above E_F : In the spectra of molecules 5 and 7, the MO is directly seen to lie above E_F , for the molecules 1 and 6 the MO is shifted above E_F for sample biases higher than the energetic positions of the charging peaks. For the molecules 2 and 4 the position of the charging peak is very close to the applied sample bias, thus their brightness is

partially increased. The molecules 3 and 8 appear dark as the energetic positions of their MOs stay below E_F at the applied imaging conditions.

In order to investigate how the charge states of neighboring molecules influence each other, we have spatially mapped the STM dI/dV and AFM frequency shift (Δf) signals for an island of molecules (Figure 5). Both channels, which were simultaneously recorded in constant-height mode at a sample bias $V_S = 2$ V, exhibit characteristic ring-like features that are associated with the charge transitions.^[25,26,34,43,48,49] The energetic position of the molecular orbitals, as well as the applied bias and the tip-sample distance, dictate for which molecules charging rings are observed and what their respective sizes are. In other words, the occurrence and the radii of the charging rings are determined by a combination of template-induced gating, tip-induced gating and screening. Both, the dI/dV and Δf vs. V_S point spectra, taken at the point marked with a red cross in the maps show sharp features, that is, charging peaks and dips (labeled “CP”), at the same energy (insets in Figure 5b,c).^[43] Analogously, the charging rings coincide for both maps (dI/dV and Δf). A larger number of charging rings can be seen in the Δf channel due to the higher long-range sensitivity of AFM compared to STM. The rings do not

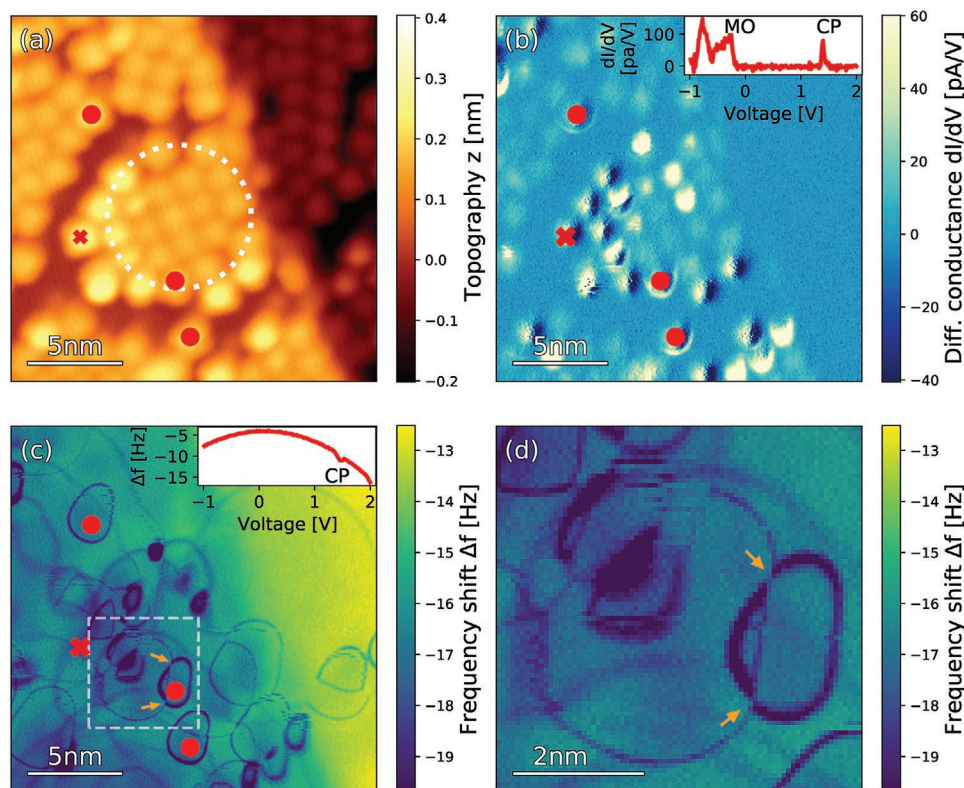


Figure 5. Simultaneous charge transition events for a high coverage sample. a) STM topography of a surface with 0.9 ML coverage. Dashed white circle marks the position of a pore area of the moiré lattice. ($V_S = 2$ V, $I = 8$ pA) b) Differential conductance (dI/dV) and c) AFM frequency shift (Δf) maps, which were simultaneously acquired in constant height mode at $V_S = 2$ V, show charging rings for certain molecules. dI/dV and Δf vs. V_S spectra (insets in (b) and (c), taken at the position marked with the red cross) show sharp features (labeled “CP”) at the same energy, which are related to charging events. ($V_S = 2$ V, $I = 5$ pA) Red dots mark positions of three molecules, the charging rings of which are visible in both maps in (b) and (c). Orange arrows in (c) mark the intersection of charging rings of two neighboring molecules. In the overlapping area the molecular orbitals of both molecules are shifted across E_F , which leads to a small contraction of the ring radii because of an increase of the charging threshold. This effect, which occurs in the area marked with the white rectangle in (c), is shown in the zoom-in in (d). The orange arrows in (c) and in (d) mark the same intersection.

exhibit a perfectly circular shape because of the asymmetry of the tip. The sizes of the rings vary—some exceed diameters of 10 nm^[48] depending on the energy position of the molecular resonances. For instance, the molecules marked with red dots exhibit relatively small charging rings that are visible in both, the dI/dV and Δf vs. V_S maps. It is interesting to investigate the intersection of charging rings, as, for example, an early STM study revealed an interaction of Ag-doping centers in an organic monolayer by dI/dV mapping of charging rings.^[25] A specific example of intersecting charging rings of neighboring molecules is marked by orange arrows in Figure 5c,d. Within the overlapping area of both charging rings, tip-induced gating changes the charge states for both molecules simultaneously, which is associated with a subtle decrease of both ring radii. This observation indicates that the charge state change of one molecule increases the charging threshold of the other molecule, shifting the CP to higher energy and thus reducing the ring radius mapped at constant tip height.

2.5. Discussion

The STM manipulation experiments presented in Figure 2 show that the level alignment of an individual molecule can be changed by lateral repositioning on the *h*-BN/Cu(111) work function template. This process is reversible. Previously, such pronounced energy shifts of MOs were mainly reported for molecular aggregates and films.^[12] Template-induced modifications of the very same molecule were only addressed by STM imaging without spectroscopic insight.^[23] The magnitude of the MO shift on *h*-BN/Cu(111) exceeds the one reported for dense-packed F₁₆CoPc arrays on graphene/Ir(111),^[50] reflecting distinct interface and template properties.^[12]

A priori, the origin and character of the MO feature is not obvious. The dI/dV spectra only reveal that the reversible tip-gating shifts the MO of F₁₆CoPc across E_F , thus changing the charge state of the molecule. Here, the sharp CP feature points to an integer charge transfer. However, the initial charge state of an individual F₁₆CoPc is not clear: An unequivocal assignment of MO-like features observed in STS measurements to specific molecular orbitals calculated for gas phase Pcs is not straightforward, for example, due to interface effects and the potential role of many-body interactions.^[19,35,51] Even with orbital-resolved STM imaging at hand (see Figure S9, Supporting Information) and restriction to a single-particle picture, the assignment is hampered by the dependence of the calculated orbital sequence on subtle details of the employed theoretical method.^[50] Nonetheless, our experimental and theoretical insights indicate that the MO signature is derived from an empty state of the free molecule, that is, the individual F₁₆CoPc accepts charge on *h*-BN/Cu(111). Specifically, our DFT calculations show that charge is readily transferred from *h*-BN/Cu(111) to F₁₆CoPc upon adsorption, yielding an anion. The calculated projected density of states reveals that a molecular orbital with strong Co d_z^2 character is fully occupied for F₁₆CoPc on *h*-BN/Cu(111) (see Figure S3, Supporting Information), whereas it is only singly occupied for the free molecule. The pronounced calculated work function increase of 0.53 eV from *h*-BN/Cu(111) (4.18 eV) to F₁₆CoPc/*h*-BN/Cu(111)

(4.71 eV) is consistent with an interfacial charge transfer from *h*-BN/Cu(111) to F₁₆CoPc.^[20,52] Experimental values reported for F₁₆ZnPc/*h*-BN/Cu(111) (0.3 eV)^[20] and F₁₆CoPc on Cu-intercalated graphene/Ni(111) (0.3 eV)^[31] show the same sign and similar magnitude for the work function difference/the interfacial dipole upon monolayer adsorption. The modifications of the STM contrast observed in the experiment are in line with this interpretation, as they point to a relevant role of electronic states centered on F₁₆CoPc. Translation of individual F₁₆CoPc units from pore toward wire regions does not change the charge state of the molecule at low bias voltage (i.e., the MO feature is observed below E_F , see Figure 2d–i, in contrast to the previously reported situation for CoPc on *h*-BN/Ir(111)^[33]). However, when imaging the molecules at bias voltages close to the CP, the brightness of the molecular center is increased (see Figure 2a–c). This can be explained by the MO becoming partially accessible to electrons tunneling from tip to sample, that is, a “tail” of the MO is shifted above E_F due to tip-induced gating. When the molecule is imaged at bias voltages above the CP, that is, in a different charge state (neutral for the individual F₁₆CoPc), the brightness of the central part of the molecule is drastically increased (e.g., see Figure 4; Figure S5, Supporting Information). A rough approximation of the interfacial energy level alignment supports the above interpretation, indicating that the MO at around 0.7 V below E_F (see Figure 2) is not likely to reflect the HOMO of the free molecule. Considering the work function of the *h*-BN/Cu(111) pore areas (experiment: 3.8 eV,^[14] DFT: 4.18 eV) and the interface dipole value listed above, one can estimate an ionization potential of about 5.4 eV. This value is clearly smaller than ionization potentials reported for F₁₆CoPc (6.15–6.4 eV).^[31,53] Interestingly, a recent study addressing F₁₆ZnPc arrays on *h*-BN/Cu(111) reveals an STS signature that is distinctly different from the F₁₆CoPc system.^[20] A pronounced resonance above E_F was assigned to the LUMO of F₁₆ZnPc, whereas no clear spectral feature is reported for occupied states.^[20] We tentatively assign this difference to the nature of the metal centers in the free molecules—closed-shell for Zn and open-shell for Co.

The effect of the local environment on the F₁₆CoPc's electronic signature as resolved by STS was modeled considering electrostatic screening of the charge (added/removed to the molecule during STS) by polarizable neighbors.^[18,54] Our model quantitatively agrees with the experimentally observed shifts of molecular resonance energies, even though additional parameters, such as the inhomogeneous charge distribution within the molecules, non-covalent intermolecular interactions, changes in adsorption geometry and distance, as well as interaction with the buried metal substrate, are not taken into account. Accordingly, this simple model captures the key findings of the experiments, in line with reports on related systems, including charged molecules on ultra-thin insulating supports.^[18,19] Additional and competing effects yielding a shift of occupied MOs toward E_F with increasing number of molecular neighbors could include incremental addition of negative charge, a change in the local work function induced by the neighboring molecules, or a Coulombic field due to surrounding charges.^[6] All these effects would shift both occupied and unoccupied molecular resonances upward (i.e., occupied MOs toward E_F , unoccupied MOs away from E_F), in contrast to

screening yielding a counter-directional shift^[19] (i.e., occupied and unoccupied MOs shift toward E_F). As many STS spectra do not provide a clear signature of the first unoccupied MO (cf. Figure 2), we have only limited information on the evolution of the $F_{16}CoPc$'s electronic gap with increasing number of neighbors. Thus, based on our experiments alone, one cannot rule out a contribution of these effects. Nonetheless, the combination of experimental STS data and DFT simulations indicates that intermolecular Coulomb interactions do not play a dominant role, as briefly discussed next. The DFT results presented in Figure S3c,d, Supporting Information, base on a chain of $F_{16}CoPc$ anions, where two adjacent molecular units are labeled A and B. Starting with a dilute chain containing only one unit (i.e., A or B) and subsequently adding the second unit (i.e., "A+B"), the respective occupied and unoccupied electronic states of the molecules are rigidly shifted upward (i.e., to higher energies). As the DFT modeling does not include screening effects, this rigid shift represents the effect of the charge of the neighboring molecules. Experimental spectra comparing molecules with only one neighbor to a molecule with three neighbors on the other hand do not show a rigid shift of the occupied and unoccupied MO, but rather a reduction of the apparent HOMO-LUMO gap (cf. Section S9, Supporting Information).

Reversible tip-induced gating resulting in CP-features in STS data of metal-organic complexes on ultra-thin spacer layers is well documented in literature.^[23–26,33,37,49] A recent report even demonstrates site-selective, field-driven charging in a molecular array adsorbed on a noble metal support.^[44] Our results show how Δf mapping can be applied to study complex situations with multiple molecules charged by the electric field of a tip. Such experiments open pathways to explore and control charging thresholds in molecular architectures.

Overall, for the investigated system and the employed scan parameters the three effects discussed—template-induced gating, tip-induced gating, and screening—can cause shifts of the measured positions of the molecular resonances in the dI/dV spectra of up to 1 V. Each of these effects contributes additively and in an approximately similar amount (~ 0.3 V) to the cumulative shift. The relative contributions of template and tip-induced gating can further be tuned by using a different substrate (such as h -BN/Ir(111)) with a larger work function modulation,^[12] as well as by a change of tip height and sample bias (under the constraints of a stable tip-sample junction). Moreover, growth of additional layers of molecules is expected to further increase the screening by molecular neighbors. The molecular response to electrostatic gating can be controlled by the adsorption height (for molecules in additional layers, as well as by chemical functionalization). Additionally, the electronic modulation in $F_{16}CoPc$ monolayers on h -BN supports might result in a spatially patterned chemical reactivity (e.g., toward small gaseous adsorbates) and can template the growth of thin molecular films, as evidenced by the nucleation of second layer $F_{16}CoPc$ in the wire regions of $F_{16}CoPc/h$ -BN/Cu(111) (Figures S7c and S8, Supporting Information). Indeed, the involvement of an orbital with strong out of plane character (Co d_z^2) in the charge transfer processes opens opportunities to control site-specific axial interactions. Furthermore, the anionic charge state for $F_{16}CoPc$ on h -BN/Cu(111) resulting from

electron transfer to the Co center reflects the characteristic electron acceptor behavior of this molecule.

3. Conclusion

In conclusion, we have investigated how the substrate templating, screening by neighboring molecules, and electrical fields between the tip and surface influence the electronic levels and charge states of $F_{16}CoPc$ on h -BN/Cu(111). Each of the three investigated parameters can induce energy shifts of up to a few hundreds meV. For the investigated system, a combination of these effects can change the charge state of certain molecules (anionic to neutral). Interestingly, switching of the charge state of a neighboring molecule was seen to exhibit a smaller effect on the charging threshold of the $F_{16}CoPc$ molecules. Such atomic scale understanding of the complex interplay of the effects of the substrate, the neighboring molecules and electric field gating is crucial for the design and utilization of molecular electronic devices, the functionalization of 2D materials, and the control of molecular nanosystems at interfaces.

4. Experimental Section

The experiments were carried out using CreaTec STM and STM/AFM machines operating at 6 K under ultra high vacuum conditions. The h -BN layer was prepared by chemical vapor deposition (CVD) using a Borazine ($HBNH_3$) precursor, which was introduced into the growth chamber through a leak valve, following a protocol described in detail in previous studies.^[12,33,55,56] The $F_{16}CoPc$ (Sigma-Aldrich, 95% purity) molecules were deposited from a quartz crucible heated to 693 K onto the h -BN/Cu(111) substrate kept at room temperature during deposition followed by a post annealing step to 423 K. The STM images were acquired in constant current mode and the differential conductance (dI/dV) spectra were recorded using the lock-in technique ($f = 969$ Hz, $\Delta V_{rms} = 20$ mV). dI/dV maps were taken in constant height mode at $f = 479$ Hz, $\Delta V_{rms} = 11$ mV unless stated otherwise. For AFM/KPFM measurements a qPlus sensor ($Q \approx 70000$, resonance frequency $f \approx 30$ kHz, $k \approx 1800$ N m^{-1} , oscillation amplitudes of 20–50 pm) was used. The data was processed using Gwyddion^[57] and Python. STM images were subjected to standard corrections, that is, plane-subtraction, as well as global brightness/contrast adjustments. A Gauss filter was applied to the the STM image in Figure 4a.

Supporting Information

Supporting Information is available from the Wiley Online Library or from the author.

Acknowledgements

M.P. and Y.W. contributed equally to this work. The authors thank P. Liljeroth for sharing DFT/PBE calculations of free $F_{16}CoPc$. This work was supported by the European Research Council Consolidator Grant NanoSurfs (No. 615233) and the Independent Research Fund Denmark through Technology and Production and Sapere Aude Research Talent program under Grant no. 4005-00311B. M.G. would like to acknowledge funding by the H2020-MSCA-IF-2014 program under GA No. 658070 (2DNano). W.A. acknowledges funding by the Deutsche Forschungsgemeinschaft via a Heisenberg professorship.

Conflict of Interest

The authors declare no conflict of interest.

Keywords

charge transfer, charging, Cu(111), F₁₆CoPc, hexagonal boron nitride, level alignment, phthalocyanines

Received: January 14, 2020

Revised: April 6, 2020

Published online: June 3, 2020

- [1] L. Lu, T. Zheng, Q. Wu, A. M. Schneider, D. Zhao, L. Yu, *Chem. Rev.* **2015**, *115*, 12666.
- [2] N. Xin, J. Guan, C. Zhou, X. Chen, C. Gu, Y. Li, M. A. Ratner, A. Nitzan, J. F. Stoddart, X. Guo, *Nat. Rev. Phys.* **2019**, *1*, 211.
- [3] P. Samori, F. Biscarini, *Chem. Soc. Rev.* **2018**, *47*, 4675.
- [4] A. Gaita-Arino, F. Luis, S. Hill, E. Coronado, *Nat. Chem.* **2019**, *11*, 301.
- [5] P. Borghetti, A. Ei-Sayed, E. Goiri, C. Rogero, J. Lobo-Checa, L. Floreano, J. E. Ortega, D. G. de Oteyza, *ACS Nano* **2014**, *8*, 12786.
- [6] A. Della Pia, M. Riello, A. Floris, D. Stassen, T. S. Jones, D. Bonifazi, A. De Vita, G. Costantini, *ACS Nano* **2014**, *8*, 12356.
- [7] J. V. Barth, *Annu. Rev. Phys. Chem.* **2007**, *58*, 375.
- [8] L. Grill, S. Hecht, *Nat. Chem.* **2020**, *12*, 115.
- [9] J. Repp, G. Meyer, *Chimia* **2010**, *64*, 370.
- [10] I. Swart, L. Gross, P. Liljeroth, *Chem. Commun.* **2011**, *47*, 9011.
- [11] A. Kumar, K. Banerjee, P. Liljeroth, *Nanotechnology* **2017**, *28*, 082001.
- [12] W. Auwärter, *Surf. Sci. Rep.* **2019**, *74*, 1.
- [13] G. Reece, N. Krane, C. Lotze, K. J. Franke, *ACS Nano* **2019**, *13*, 7031.
- [14] S. Joshi, F. Bischoff, R. Koitz, D. Ecija, K. Seufert, A. P. Seitsonen, J. Hutter, K. Diller, J. I. Urgel, H. Sachdev, J. V. Barth, W. Auwärter, *ACS Nano* **2014**, *8*, 430.
- [15] J. B. Neaton, M. S. Hybertsen, S. G. Louie, *Phys. Rev. Lett.* **2006**, *97*, 216405.
- [16] I. Fernandez-Torrente, K. J. Franke, J. I. Pascual, *J. Phys.: Condens. Matter* **2008**, *20*, 184001.
- [17] M. Hollerer, D. Lüftner, P. Hurdax, T. Ules, S. Soubatch, F. S. Tautz, G. Koller, P. Puschnig, M. Sterrer, M. G. Ramsey, *ACS Nano* **2017**, *11*, 6252.
- [18] K. A. Cochrane, A. Schiffrin, T. S. Roussy, M. Capsoni, S. A. Burke, *Nat. Commun.* **2015**, *6*, 8312.
- [19] K. A. Cochrane, T. S. Roussy, B. Yuan, G. Tom, E. Marsell, S. A. Burke, *J. Phys. Chem. C* **2018**, *122*, 8437.
- [20] A. Tan, P. P. Zhang, *Phys. Chem. Chem. Phys.* **2019**, *21*, 26146.
- [21] A. Riss, S. Wickenburg, L. Z. Tan, H.-Z. Tsai, Y. Kim, J. Lu, A. J. Bradley, M. M. Ugeda, K. L. Meaker, K. Watanabe, T. Taniguchi, A. Zettl, F. R. Fischer, S. G. Louie, M. F. Crommie, *ACS Nano* **2014**, *8*, 5395.
- [22] S. Wickenburg, J. Lu, J. Lischner, H. Tsai, A. A. Omrani, A. Riss, C. Karrasch, A. J. Bradley, H. S. Jung, R. Khajeh, D. Wong, K. Watanabe, T. Taniguchi, A. Zettl, A. H. C. Neto, S. G. Louie, M. F. Crommie, *Nat. Commun.* **2016**, *7*, 13553.
- [23] L. Liu, T. Dienel, R. Widmer, O. Gröning, *ACS Nano* **2015**, *9*, 10125.
- [24] I. Swart, T. Sonleitner, J. Repp, *Nano Lett.* **2011**, *11*, 1580.
- [25] G. V. Nazin, X. H. Qiu, W. Ho, *Phys. Rev. Lett.* **2005**, *95*, 166103.
- [26] V. W. Brar, R. Decker, H.-M. M. Solowan, Y. Wang, L. Maserati, K. T. Chan, H. Lee, C. O. Girit, A. Zettl, S. G. Louie, M. L. Cohen, M. F. Crommie, *Nat. Phys.* **2011**, *7*, 43.
- [27] L. Grill, *J. Phys.: Condens. Matter* **2008**, *20*, 053001.
- [28] H. Peisert, M. Knupfer, T. Schwieger, G. G. Fuentes, D. Olligs, J. Fink, T. Schmidt, *J. Appl. Phys.* **2003**, *93*, 9683.
- [29] H. Peisert, J. Uihlein, F. Petraki, T. Chassé, *J. Electron. Spectrosc.* **2015**, *204*, 49.
- [30] F. Ruckerl, D. Waas, B. Büchner, M. Knupfer, *J. Electron. Spectrosc.* **2017**, *215*, 1.
- [31] D. Balle, H. Adler, P. Grüninger, R. Karstens, R. Ovsyannikov, E. Giangrisostomi, T. Chassé, H. Peisert, *J. Phys. Chem. C* **2017**, *121*, 18564.
- [32] I. Fernandez-Torrente, D. Kreikemeyer-Lorenzo, A. Strozecka, K. J. Franke, J. I. Pascual, *Phys. Rev. Lett.* **2012**, *108*, 036801.
- [33] F. Schulz, R. Drost, S. K. Hämäläinen, P. Liljeroth, *ACS Nano* **2013**, *7*, 11121.
- [34] N. Hauptmann, C. Hamann, H. Tang, R. Berndt, *Phys. Chem. Chem. Phys.* **2013**, *15*, 10326.
- [35] F. Schulz, M. Ijäs, R. Drost, S. K. Hämäläinen, A. Harju, A. P. Seitsonen, P. Liljeroth, *Nat. Phys.* **2015**, *11*, 229.
- [36] G. V. Nazin, S. W. Wu, W. Ho, *Proc. Natl. Acad. Sci.* **2005**, *102*, 8832.
- [37] S. W. Wu, G. V. Nazin, X. Chen, X. H. Qiu, W. Ho, *Phys. Rev. Lett.* **2004**, *93*, 236802.
- [38] M. Schwarz, D. A. Duncan, M. Garnica, J. Ducke, P. S. Deimel, P. K. Thakur, T.-L. Lee, F. Allegretti, W. Auwärter, *Nanoscale* **2018**, *10*, 21971.
- [39] A. Mehler, N. Néel, J. Kröger, *J. Vac. Sci. Technol. A* **2019**, *37*, 061404.
- [40] M. Schwarz, A. Riss, M. Garnica, J. Ducke, P. S. Deimel, D. A. Duncan, P. K. Thakur, T. L. Lee, A. P. Seitsonen, J. V. Barth, F. Allegretti, W. Auwärter, *ACS Nano* **2017**, *11*, 9151.
- [41] K. Teichmann, M. Wenderoth, S. Loth, R. G. Ulbrich, J. K. Garleff, A. P. Wijnheijmer, P. M. Koenraad, *Phys. Rev. Lett.* **2008**, *101*, 076103.
- [42] P. Järvinen, S. K. Hämäläinen, K. Banerjee, P. Häkkinen, M. Ijäs, A. Harju, P. Liljeroth, *Nano Lett.* **2013**, *13*, 3199.
- [43] N. Kocic, P. Weiderer, S. Keller, S. Decurtins, S. X. Liu, J. Repp, *Nano Lett.* **2015**, *15*, 4406.
- [44] D. Kumar, C. Krull, Y. Yin, N. V. Medhekar, A. Schiffrin, *ACS Nano* **2019**, *13*, 11882.
- [45] R. Ramprasad, N. Shi, *Appl. Phys. Lett.* **2006**, *88*, 222903.
- [46] O. T. Hofmann, P. Rinke, M. Scheffler, G. Heimel, *ACS Nano* **2015**, *9*, 5391.
- [47] P. Scheuerer, L. L. Patera, J. Repp, *Nano Lett.* **2020**, *20*, 1839.
- [48] L. Cockins, Y. Miyahara, S. D. Bennett, A. A. Clerk, S. Studenikin, P. Poole, A. Sachrajda, P. Grutter, *Proc. Natl. Acad. Sci.* **2010**, *107*, 9496.
- [49] N. A. Pradhan, N. Liu, C. Silien, W. Ho, *Phys. Rev. Lett.* **2005**, *94*, 076801.
- [50] P. Järvinen, S. K. Hämäläinen, M. Ijäs, A. Harju, P. Liljeroth, *J. Phys. Chem. C* **2014**, *118*, 13320.
- [51] C. Uhlmann, I. Swart, J. Repp, *Nano Lett.* **2013**, *13*, 777.
- [52] H. Cun, A. P. Seitsonen, S. Roth, S. Decurtins, S.-X. Liu, J. Osterwalder, T. Greber, *Surf. Sci.* **2018**, *678*, 183.
- [53] M. Toader, T. G. Gopakumar, P. Shukryna, M. Hietschold, *J. Phys. Chem. C* **2010**, *114*, 21548.
- [54] R. Hesper, L. H. Tjeng, G. A. Sawatzky, *Europhys. Lett.* **1997**, *40*, 177.
- [55] S. Joshi, D. Ecija, R. Koitz, M. Iannuzzi, A. P. Seitsonen, J. Hutter, H. Sachdev, S. Vijayaraghavan, F. Bischoff, K. Seufert, J. V. Barth, W. Auwärter, *Nano Lett.* **2012**, *12*, 5821.
- [56] W. Auwärter, T. J. Kreuz, T. Greber, J. Osterwalder, *Surf. Sci.* **1999**, *429*, 229.
- [57] D. Necas, P. Klapetek, *Open Phys* **2012**, *10*, 181.